Journal of Radioanalytical and Nuclear Chemistry (2023) 332:63–76
https://doi.org/10.1007/s10967-022-08669-4

Inclusion, occlusion and adsorption of rare earth elements from chloride media onto barite-gypsum composite

Sh. M. Abdo[1] · M. S. Hagag[1] · A. H. Ali[1] · F. H. Salem[1] · G. A. Dakroury[2]

Received: 31 July 2022 / Accepted: 11 November 2022 / Published online: 23 December 2022

Abstract

In this study, a synthetic $BaSO_4$·$CaSO_4$ composite was prepared by co-precipitation technique, characterised and examined for REE sorption. The sorption parameters were; pH = 4, equilibrium time = 20 min, temperature = 303 K, and REE liquor volume to composite mass ratio of 0.2:1 L g^{-1}. The sorption reaction was controlled by pseudo 2nd order kinetic mechanism and Langmuir adsorption isotherm with an adsorption capacity of 168.63 mg g^{-1}. 90.14% of REE (III) was desorbed using 1 mol L^{-1} HNO_3. The process was endothermic and spontaneous. Accordingly, 1:1 barite-gypsum (natural ingredient for $BaSO_4$·$CaSO_4$), with 136 mg g^{-1} loading capacity, was used for REEs extraction.

Keywords Gypsum · Barite · Rare earth elements · Sorption

Introduction

Rare earth elements REEs are elements of the 4f sub-level, consisting of 15 elements, besides scandium and yttrium, although they belong to the first and second transition elements [1]. Because REEs are widely used in many important fields, such as magnetic, optical, and electrical properties, scientists are working to extract and separate REEs from their ores. REEs have nearly identical atomic radii in the range of 0.87 to 1.25 A°, which is the controlling factor for their similarity in chemical and physical properties, making individual separation difficult and costly [2]. REEs are located in all types of rocks: igneous, sedimentary, and metamorphic rocks [3]. Nevertheless, the main REE resources are monazite (one of the black sand ingredients), bastnaesite, parisit, euxenit, loparit, xenotime [4], and phosphate. In Egypt, the main REE resource is monazite, which is extensively ascertained at the northern cost of the Mediterranean Sea but limited to the southern coast of the Red Sea [5]. Many chemical methods have been used to separate REEs from their ores or leach liquors, including precipitation [6], solvent extraction [7], ion-exchange [8], adsorption [9], liquid emulsion membrane [10, 11], and ion inclusion membrane [12]. Generally, precipitation methods (through double-sulfate or HF or oxalic acid as a precipitate) are probably applied at REE concentrations of more than 10%, whereas solvent extraction methods are performed at concentrations of > 2000 mg L^{-1}. Finally, ion-exchange and adsorption methods are preferred at concentrations of 1000 mg L^{-1} [13–20]. The sorption process is the transfer of adsorbate ions from an aqueous solution to the adsorbent (solid phase) across the boundary between the two phases. Recently, adsorption has been extensively used in scientific research and industrial applications for multiple purposes, including separation of valuable elements and compounds, purifications, and removal of heavy metals and pollutants [21–24]. Ion-exchange is mainly chemisorptions in nature due to the exchange of ions between the liquid and solid phases. In addition, the chemical energy before ionic exchange is higher than that after the exchange process, whereas the adsorption process includes two types of sorption: chemisorptions and physisorption [25]. REEs adsorptions are complemented by many adsorbents that vary in performance, uptake, pH range, and selectivity. Many adsorbents have been utilised for REE separations, including ores (clay minerals, kaolinite, soil, and halloysite) [26–28], hyper composites (β-cyclodextrin and silica doped with PC88A [29], composite (graphene oxide-tris (4-aminophenyl) amine) [30], polymer composite P(AA-co-AM/PJM-T)

✉ G. A. Dakroury
dr_gdakrory2010@yahoo.com

[1] Nuclear Materials Authority, P.O 530 Maadi, Cairo, Egypt

[2] Nuclear Chemistry Department, Hot Laboratories Centre, Egyptian Atomic Energy Authority, P.O. 13759, Cairo, Egypt

[31], metal–organic framework (novel DGA-functionalized metal organic frameworks) [32], zeolite (zeolitic imidazolate frameworks) [33], biomass (Phosphorylated Hydrogel (Algal Biomass PEI) [34], and lignocelluloses biomass based on banana waste) [35] and waste material (phosphogypsum) [15]. Authors [36–38] investigated the possibility of extracting REEs through the recycling of low value waste streams such as bauxite residue, mine tailings, PG, slag and waste waters. However, there is no study of the separation of REEs from their ores by barite-gypsum composite.

Barite (barium sulphate; $BaSO_4$) is an important inorganic compound used in painting, coating, plastics and pharmaceuticals fibre. The efficient removal of Ra(II) using $BaSO_4{\cdot}SrO_4$ by co-precipitation of Ra-Ba-SO_4 attributed to the rapid $BaSO_4$ nucleation rate [39], closer ionic radii of Ra(II) with Ba(II) and experimental studies revealed that divalent cations (i.e., Mg(II), Ca(II), Sr(II) and Ba(II)) have significantly higher impact on radium removal by barite than monovalent cations.

Herein, authors decided to examine synthetic $BaSO_4{\cdot}CaSO_4$ to separate REEs from the acidic chloride leach liquor of monazite mineral (150 meshes) and apply the optimum conditions for REE separation from monazite by synthetic $BaSO_4{\cdot}CaSO_4$ onto natural 1:1 barite-gypsum composite.

This paper included the preparation of synthetic ($BaSO_4{\cdot}CaSO_4$) composite by co-precipitation of barium sulphate and calcium sulphate (the main constituents for barite and gypsum) for the separation of REEs from acidic chloride leach liquor of monazite mineral (150 meshes). The characterization of the prepared composite was carried out by FT-IR, XRD, DTA, SEM, particle size analysis, and pore size distribution. All adsorption and desorption behaviours were well studied, in addition to adsorption isotherms, adsorption kinetics, adsorption mechanisms, and even regeneration and reusability. It is well expected that the prepared adsorbent (mixed sulphate) has extremely high resistance to all mineral acid attacks based on the anionic radical (sulphate), which is never replaced with any anionic radial of the other mineral acids, besides the low solubility product of calcium and barium sulphate. Finally, the optimised adsorption conditions were applied to barite-gypsum composite as a cheap sorbent prepared from natural ores. Eventually, this work conducted a novel bio-adsorbent that has high work ability, including high resistance to extreme acidic conditions and reusability.

Materials and methods

Preparation of $BaSO_4{\cdot}CaSO_4$ sorbent

At 30 °C, an equivalent amount of $BaCl_2.2H_2O$ and $CaCl_2.2H_2O$ salts are vigorously mixed with distilled water until completely dissolved [40]. Finally, add the dissolved $BaCl_2.2H_2O$ and $CaCl_2.2H_2O$ mixtures to Na_2SO_4. A white precipitate forms immediately, which was separated by filtration. The co-precipitated calcium sulphate and barium sulphate were dried at 100 °C for 3 h.

$CaCl_2.2H_2O$ and $BaCl_2.2H_2O$ were co-precipitated according to the two following reactions:

$$\mathrm{Ca\ (II)} + \mathrm{SO_4(II)} + 2\mathrm{H_2O} \rightarrow \mathrm{CaSO_4.2H_2O} \quad (1)$$

$$\mathrm{Be\ (II)} + \mathrm{SO_4(II)} + 2\mathrm{H_2O} \rightarrow \mathrm{BaSO_4\boxed{人}2H_2O} \quad (2)$$

Preparation of REE solutions

In a 50 cc solution of concentrated HCl acid, REEs hydroxide cake, (obtained from monazite digestion), was carefully dissolved in an 85 °C water bath [31]. Different REE concentrations were created for each batch experiment trial by diluting the stock standard solution, which had an initial concentration of 2000 mg L^{-1}.

Instruments

The active functional groups in the $BaSO_4{\cdot}CaSO_4$ composite were identified using a Bomen Miclson FT-IR spectrophotometer, model MB157 from Canada. Shimadzu x-ray diffraction (XRD); model XD-Dl, Kyoto, Japan, with a diffraction angle (2θ) range of 4–70°, was used to identify the crystalline phase structure. The Japanese DTA-TGA-50 maintains thermal stability at a constant rate of 5 °C/min from room temperature to 650 °C. The particle morphology was investigated using a JEOL JSM-5400 (SEM, FEI Quanta FEG-250, and EDX) for SEM and EDX mapping. The pore-size chromatech 9320, USA, was used to determine the pore size distribution and its corresponding porosity. The UV-spectrophotometer (SP-8001) and the Inductive Coupled Plasma Optical Emission Spectrometer (Prodig Axial high dispersion ICP-OES model, USA) were used to measure the concentration of rare earth ions. However, the concentration of calcium ions was measured by an atomic absorption spectrophotometer (Buck Scientific, VGP 210).

Sorption studies

The sorption technique was employed to extract REE (III) ions from monazite ore. Batch studies were conducted to inspect the sorption performance of REE onto $BaSO_4{\cdot}CaSO_4$ composite. The impact of [H^+] concentration (10^{-2}–10^{-5}), time (15–120) minutes, REE(III) volume to composite mass ratio (0.1–0.4), initial REE (III) concentration (200–2000 mg L^{-1}) and temperature were discussed. After contacting 0.1 g of $BaSO_4{\cdot}CaSO_4$ composite with 20 mL of

REE (III) solution, samples were separated from the solution by filtration.

Equation (3) gives the sorption efficiency (%) of REE (III) at each time interval [41].

$$\text{Sorption efficiency (\%)} = \left(\frac{C_i - C_f}{C_i}\right).100 \quad (3)$$

Adsorbed amount q (mg g^{-1}) is calculated using Eq. (4) [41]:

$$q = \left(\frac{C_i - C_f}{C_i}\right).\frac{V}{m} \quad (4)$$

where, q denotes the sorbed amount (mg g^{-1}). The initial and final concentrations of the REE (III) are denoted by C_i and C_f, respectively. The weight of the $BaSO_4{\cdot}CaSO_4$ (g) is denoted by m. (g), where V denotes the volume of solution (L).

Equation (5) gives the distribution coefficient K_d [42]

$$K_d = \left(\frac{C_i - C_f}{C_f}\right).\frac{V(mL)}{m(g)} \quad (5)$$

Kinetic modelling

Using kinetic modelling and selecting the appropriate one for the sorption reaction, the mechanism of the sorption reaction could be proposed. This study employs four kinetics models: pseudo first order, pseudo second order, the Elovich model, and the intra-particle diffusion model.

Pseudo first order and pseudo second order models

Equations (6) and (7) give the linear equations of pseudo-first order equation [41] and pseudo second order [43], respectively.

$$Log\left(q_e - q_t\right) = \log q_e - \frac{k_1}{2.303}t \quad (6)$$

$$\frac{t}{q_t} = \frac{1}{k_2 q_e^2} + \frac{1}{q_e}t \quad (7)$$

where q_e and q_t are the sorbed amounts of REE (III) at equilibrium time and any time t, respectively, k_1 (min^{-1}) and k_2 (g mg^{-1}) express the rate constants of pseudo first order and pseudo second order, respectively.

Elovich model

It describes chemisorptions reactions and could be calculated using Eq. (8) [41].

$$qt = \frac{1}{\beta}\ \ln(\alpha\beta) + \frac{1}{\beta}\ \ln t \quad (8)$$

where α and β represent Elovich parameters. α (mg g^{-1} min^{-1}) represents the initial adsorption rate and β expressed desorption rate constant (g mg^{-1}).

Intra-particle diffusion model

Equation (9) [44] is used to apply the intra-particle diffusion model.

$$q_t = K_{id}t^{0.5} + C \quad (9)$$

where k_{id} represents the rate constant of intra-particle diffusion (mg g^{-1} $min^{-1/2}$) and C represents the intercept.

Isotherm Modellin

This study employs four isotherm models: Langmuir [45], Freundlich [46], and Halsey [47], and Temkin isotherm [48].

Langmuir and Freundlich model

Langmuir isothermes model examined using linear form Eq. (10)

$$\frac{C_e}{q_e} = \frac{1}{bQ_o} + \frac{1}{Q_o}C_e \quad (10)$$

where Q_o is the Langmuir adsorption capacity (mg g^{-1}), b is the constant related to ΔG^o ($b\ \alpha\ e^{-\Delta GRT}$), and C_e is the equilibrium metal ion concentration.

The separation factor R_L could be calculated using Eq. (11)

$$R_L = \frac{1}{1 + bC_o} \quad (11)$$

C_o denotes the initial adsorbate concentration (mg g^{-1}). Adsorption is unfavourable when $R_L > 1$, linear when $R_L = 1$, favourable when $R_L = 1$, and irreversible when $R_L = 0$.

While the linear regression for the Freundlich model is given by Eq. (12)

$$\log q_e = \log K_f + \frac{1}{n}\log C_e \quad (12)$$

where K_f is the Freundlich constant and n is the adsorption capacity and intensity.

Halsey model

The Halsey model applied using Eq. (13) [47]

$$q_e = \frac{1}{n_H} \ln K_H + \frac{1}{n_H} \ln C_e \quad (13)$$

where k_H and n are the Halsey isotherm constant and exponent, respectively. This model applied for multilayer adsorption and heterogonous nature of the adsorbent.

Temkin model

The linear regression of Temkin is given by Eq. (14) [48]

$$q_e = B_T \ln A_T + B_T \ln C_e \quad (14)$$

where: $B_T = \frac{RT}{b_T}$ Where, A_T, B_T *are* constants, A_T (L mol^{-1}) is related to the maximum binding energy, b_T is said to be the adsorption heat.

Desorption studies

The loaded $BaSO_4{\cdot}CaSO_4$ by REE was desorbed in several desorbing agents for an hour. The mixture was filtrate to separate the $BaSO_4{\cdot}CaSO_4$.composite from the liquid phase, and then the concentration of REE ions measured. The desorption efficiency % was calculated using Eq. (15):

$$\text{Desorption } \% = \frac{C_{aq}}{C_s} \% \quad (15)$$

where C_{aq} is assigned to the concentration of REE within the aqueous phase C_s is that the concentration of REE within the $BaSO_4{\cdot}CaSO_4$.

Result and discussion

Characteristics f the adsorbent

FTIR analysis

Figure 1 showed the characteristics peaks for the present functional groups of $BaSO_4{\cdot}CaSO_4$ composite and after loading with REE (III). The observed wave numbers weree 3610, 3552 and 1622 cm^{-1} corresponding to stretching band of water molecule. Theses hydroxyls ion increased the Ca (II) exchange with REE (III) [49]. While in loaded $BaSO_4{\cdot}CaSO_4$ composite the peaks at 1146, 1084 and 983 cm^{-1} in $BaSO_4{\cdot}CaSO_4$ assigned to symmetrical vibration of SO_4^{2-} were shifted to 1128, 1075 and 982 cm^{-1}. However, due to deformation structure after REE (III) loading. The band at 2135 cm^{-1} corresponded to the sulphur-oxygen stretching vibration is changed to the bending vibration of SO_4^{2-} and shifted to 2064 cm^{-1}. The two peaks at 2925, 2855 cm^{-1} related to the symmetric and asymmetric vibration of SO_4^{2-} [50].

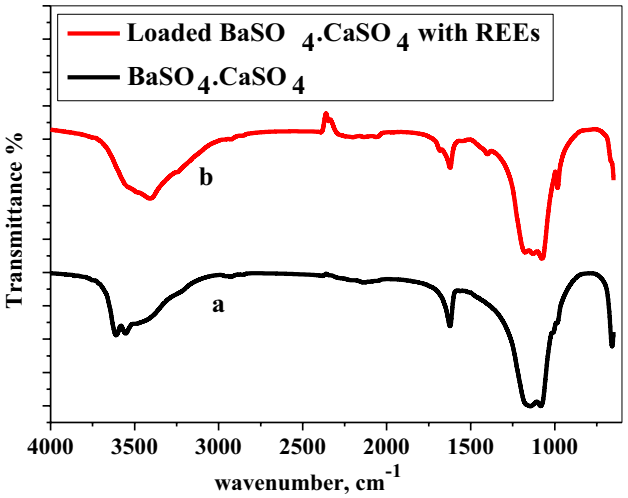

Fig. 1 FTIR analysis of (a) $BaSO_4{\cdot}CaSO_4$ composite (b) Loaded $BaSO_4{\cdot}CaSO_4$ composite with REEs

SEM analysis, EDX and Particle size distribution

Figure 2A, b described the SEM photograph of $CaSO_4{\cdot}BaSO_4$ composite before and after loading with REE. Figure 2a clarified the material has crystalline properties as the particles have a definite and regular shape. The morphology of the composite powder is polycrystalline. The grain size observed is ~ less than 1 µm. Two different regions are identified, the white agglomerated particles referred to flower shaped of $BaSO_4$ respectively [51]. However, the grey agglomerated particles referred to spherical particles of $CaSO_4$ [52]. Figure 2b showed rough surface and REEs adhered to the surface of the composite as indicated by arrows. Figure 2c represented the difference in fine particle [53] size of $BaSO_4{\cdot}CaSO_4$ composite (500 < particle size < 1300 nm) before and after sorption. The particle size of $BaSO_4{\cdot}CaSO_4$ composite increases after sorption process, which may be attributed to the agglomeration of the particles or to sorption of REE(III). The EDX mapping of $BaSO_4{\cdot}CaSO_4$ composite after sorption was represented in Fig. 2d, where REE(III) are adequately adsorbed at the surface of the composite and are distributed uniformly. La, Ce, Sm, Eu and Gd are taken as examples of REEs.

Thermal analysis

Figure 3 depicts the thermal stability of $BaSO_4{\cdot}CaSO_4$ composite. The prepared composite shows great thermal stability. As shown in Fig. 3, the total weight loss up to 700 °C was 3.93%, accompanied by three endothermic peaks at 132 °C, 205 °C, and 340 °C. The first endothermic peak is due to loss of physically adsorbed water, with a weight loss 3.51%. While the second and third endothermic peaks were

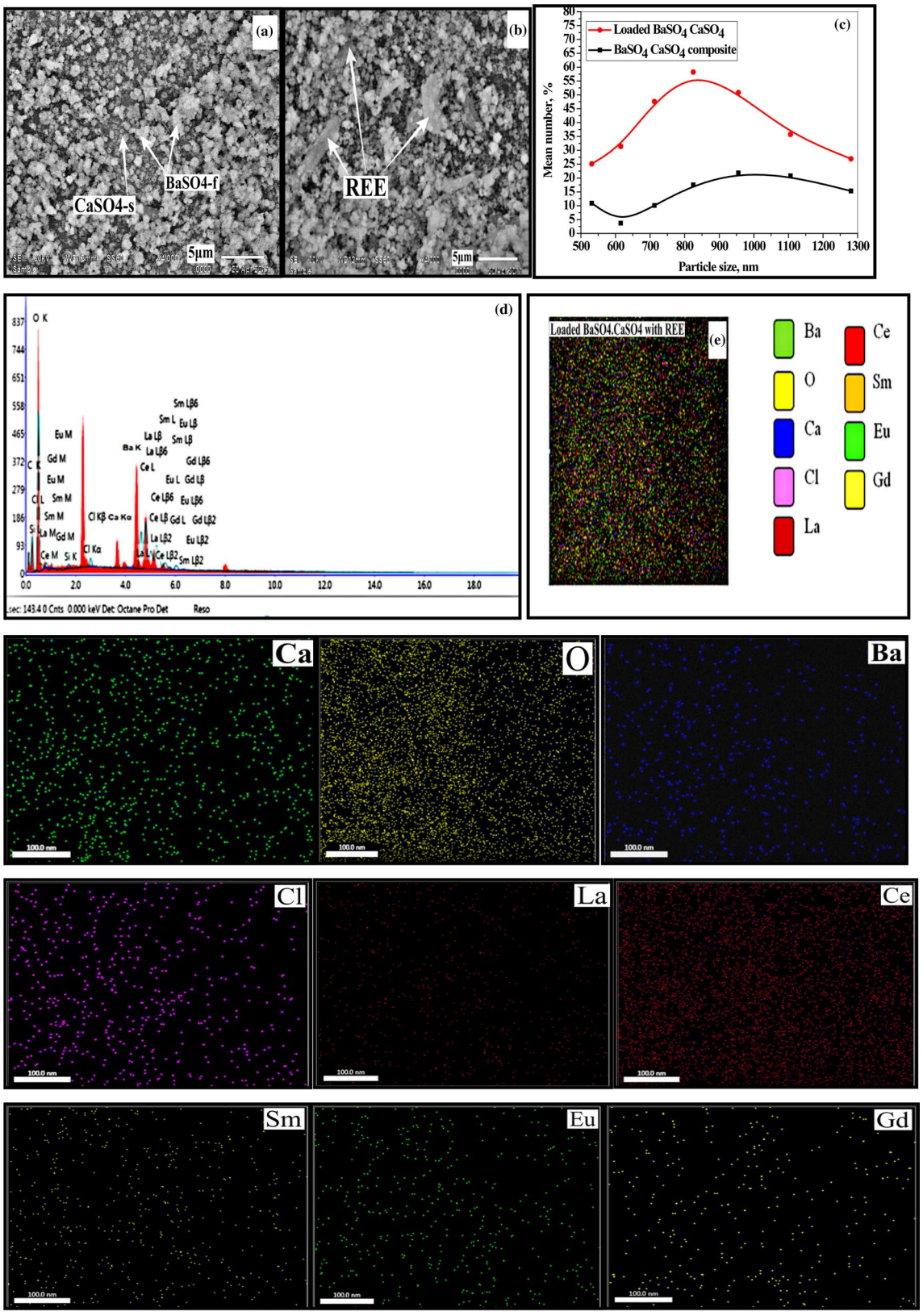

Fig. 2 SEM of (a) $BaSO_4$·$CaSO_4$ composite (b) Loaded $BaSO_4$·$CaSO_4$ composite with REEs (c) Particle size distribution (d), (e) EDX mapping of loaded $BaSO_4$·$CaSO_4$ composite with REEs

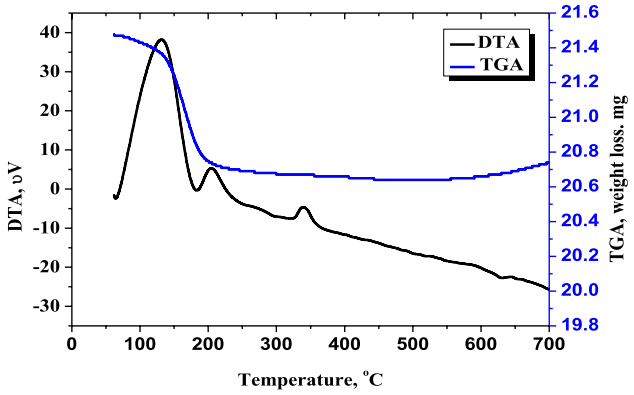

Fig. 3 TG–DTA of $BaSO_4$·$CaSO_4$ composite

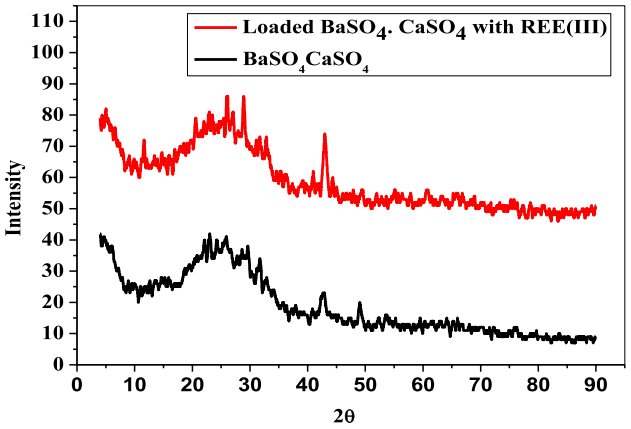

Fig. 4 X-ray diffraction of $BaSO_4$·$CaSO_4$ composite

at 205 °C and 340 °C with a total weight loss 0.42% due to removal of the structural water from $BaSO_4$ and $CaSO_4$ [54].

Surface measurements

The surface parameters of the $BaSO_4$·$CaSO_4$ composite can be seen at Table 1. The total pore area increase due to the roughness of the surface increases after REE (III) sorption [55]. However, the average pore diameter decreased due to packing of REE (III) ions on the inner wall of pore in the sorption process, resulting in a decrease in the total pore volume. The bulk density expresses the volume of the $BaSO_4$·$CaSO_4$ composite and closed pores. While the apparent density expresses the volume of the $BaSO_4$·$CaSO_4$ composite, closed pores and open pores, comparing the two densities for $BaSO_4$·$CaSO_4$ composite before sorption and after sorption, it is clear that, the open pores decreases after sorption process and a prediction for intra-particle diffusion mechanism fitting is considered.

X-ray diffraction

Figure 4 showed the XRD-pattern of $BaSO_4$ $CaSO_4$ before and after loading with REE (III). The most intense amorphous broad peak located at $2\theta = 25.9^{o}$ corresponding to $BaSO_4$, was present in the two diffracting gram. A shift in the peaks from at $2\theta = 29.59^{o}$ to 28.89^{o} and from at $2\theta = 49.06^{o}$ to 42.96^{o} could be attributed to the insertion of REE^{3+} in the $BaSO_4$ $CaSO_4$ lattice.

Sorption studies

pH impact

Sorption of REE (III) was highly affected by the change of $[H^+]$. Investigations were performed by changing pH from (1–5) and the results represented in Fig. 5a. It was observed that, as the $[H^+]$ concentration decreased, the sorption efficiency increased. This is due to [the competition of $[H^+]$ to REE (III) for the active sites of $BaSO_4$.$CaSO_4$ composite. The maximum sorption capacity was found to be at pH 4. At pH 5, it was noticed that an increase of sorption capacity, but these increase owing to the formation of several hydroxides of REE (III) [56]. This result was confirmed by precipitation curve Fig. 5b. However, Shukla et al. [57] reported that the decrease in pH value below pH 2.5 caused an increase in the solubility of $CaSO_4$ due to higher hydration of ions. Therefore, pH 4 selected as an optimum pH for the experimental batch sorption reaction.

Time impact

Figure 6 investigated that the time impact on the sorption reaction. The reaction between REE (III) and $BaSO_4$·$CaSO_4$ composite firstly was rapid due to the increased number of available vacant sites [58]. It then became slower till it reached the equilibrium at 20 min due to slower mass transfer from the bulk of the solution to the surface of the composite as the concentration of REE (III) decrease [59]. After

Table 1 Surface parameters of $BaSO_4$·$CaSO_4$ composite and loaded $BaSO_4$·$CaSO_4$ with REE (III)

Sorbent	Total pore area (m^2g^{-1})	Average pore diameter (nm)	Bulk density (g mL^{-1})	Apparent density (g mL^{-1})	Porosity (%)
$BaSO_4$·$CaSO_4$	12.25	212	0.83	1.79	53.82
Loaded $BaSO_4$·$CaSO_4$	54.27	53.6	0.89	0.54	39.35

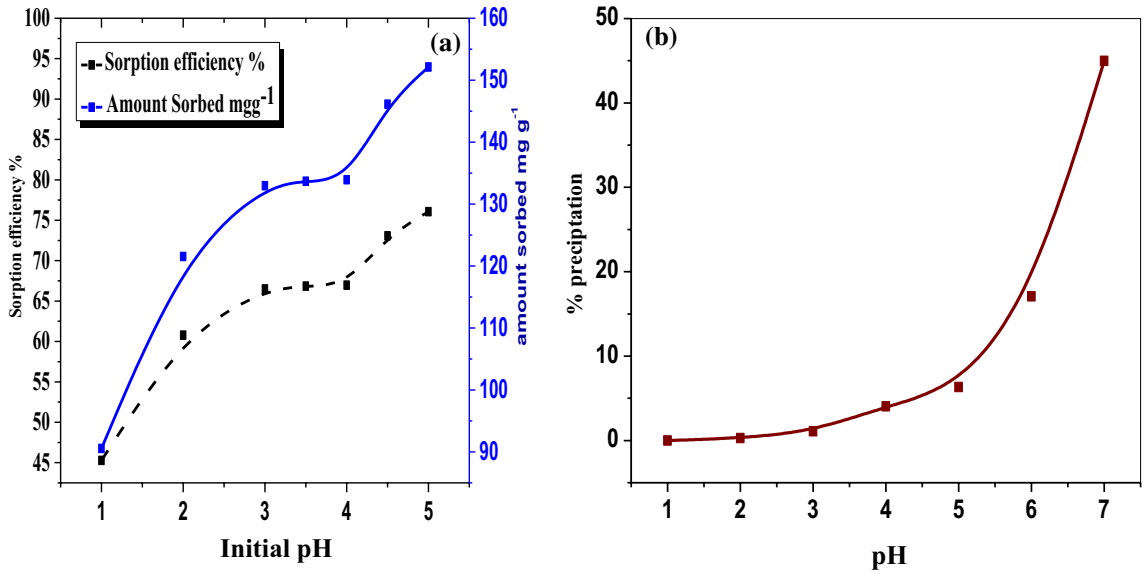

Fig. 5 pH impact of sorption of REE (III) onto $BaSO_4$·$CaSO_4$ composite [$C_o = 1000$ mg g^{-1}, Time = 24 h, v/m = 0.2 L g^{-1} and Temp. = 303 K]

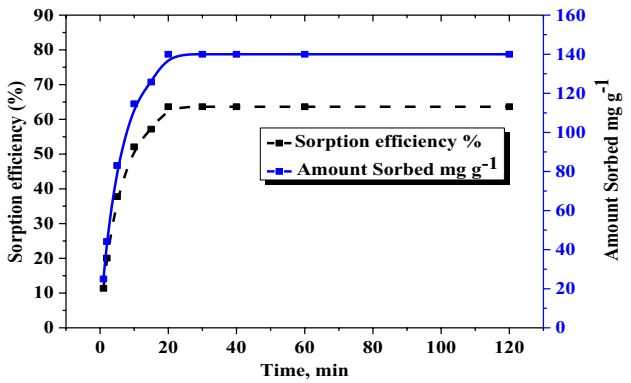

Fig. 6 Time impact of sorption of REE (III) onto $BaSO_4$·$CaSO_4$ composite [$C_o = 1100$ mg g^{-1}, pH = 4, v/m = 0.2 L $g^{-1}$and Temp. = 303 K]

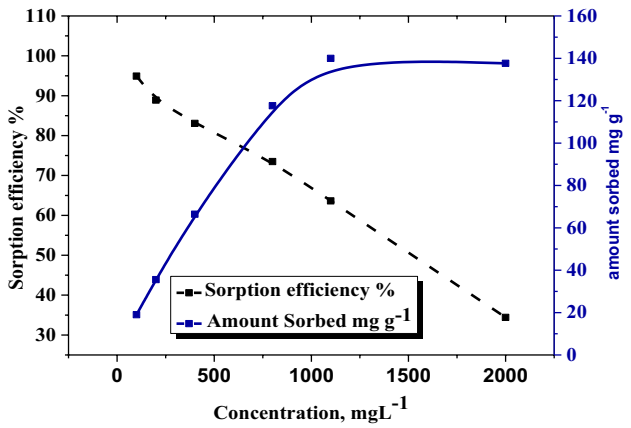

Fig. 7 Metal Ion concentration impact of sorption of REE (III) onto $BaSO_4$·$CaSO_4$ composite [Time = 20 min, pH = 4, v/m = 0.2 L $g.^{-1}$ and Temp. = 303 K]

equilibrium time, no further increase in the sorbed amount due to the saturation state and the available active sites filled by REE (III). The equilibrium concentration of REE (III) into $BaSO_4$·$CaSO_4$ composite was 140 mg g^{-1}.

Concentration impact

The impact of initial metal concentration had a great influence on the sorption reaction. Figure 7 depicted the sorption efficiency and the sorbed amount as a function of initial concentration. It was observed that at lower initial concentration of 100 mg L^{-1}; the sorption efficiency and sorbed amount were 94.92% and 18.98 mg L^{-1}, respectively. While, at higher initial concentration of 2000 mg L^{-1}, the sorption efficiency and sorbed amount were 34.41% and 137.64 mg L^{-1}, respectively. This behaviour was explained by the available free active sites at lower initial concentration [60], while an increase in initial REE(III) concentration implies that REE(III) ions were present in the mixture and hence more ions were attached to same quantity of the active sites of $BaSO_4$·$CaSO_4$ composite in addition to the increase in the driving force for the movement of the REE(III) ions from the mixture to the composite surface and, in this case, higher concentration would result in sorbent surface saturation [61].

Temperature impact

The temperature effected the sorption reaction due to its relationship with the kinetic energy of metal ions in the solution [59]. Figure 8 investigated the temperature as a

function of the sorbed amount (q_e) and distribution coefficient (K_d). The temperature impact was studied at a temperature range of 30–50 °C. It was shown that as the temperature increased, both of the sorbed amount and distribution coefficient increased due to the increase in kinetic energy i.e. the increase of the accessibility of REE (III) onto active sites of $BaSO_4$·$CaSO_4$ composite pointed to the endothermic nature of the sorption process.

The sorbed amounts of REE (III) onto $BaSO_4$·$CaSO_4$ composite were 140, 163.38 and 180.37 mg g^{-1} at 30, 40, and 50 °C, respectively.

V/m ratio Impact

Figure 9 depicted the effect of the V/m ratio on sorption of REE(III) onto $BaSO_4$·$CaSO_4$ composite. 0.1 g of $BaSO_4$·$CaSO_4$ composite was contacted with different volumes of REE(III); 10, 20, 30, and 40 ml. The results illustrated an increase in sorption efficiency and sorbed amount at v/m ratios 0.1 and 0.2. After these ratios any extra increase leaded to a decrease in sorption efficiency and sorbed amount. This is because there are enough vacant active sites available for binding till the 0.2 V/m ratios and by increasing the V/m ratios the REE (III) ions increased but the active sites did not.[62].

Kinetic Modelling

With the aid of Eqs. (4–6), the kinetic modelling was inspected; pseudo-1st – order, pseudo-2nd—order, intra particle diffusion model and Elvoich model. S.1 a, b, c, and d showed the linear regression of the applied models of REE(III) sorption onto $BaSO_4$·$CaSO_4$ composite, and Table 2 listed its estimated parameters. It is evident that the value of the R^2 for the pseudo-2nd -order and pseudo

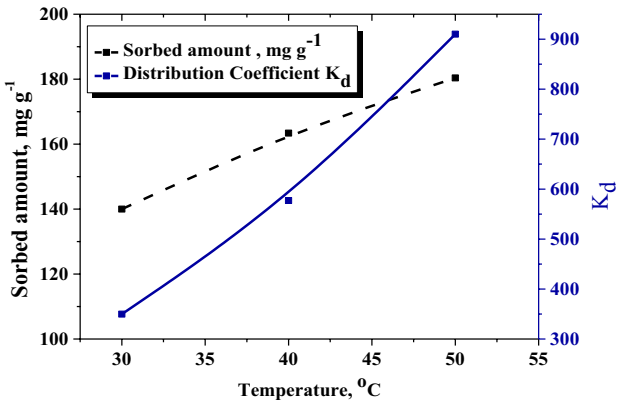

Fig. 8 Temperature impact of sorption of REE (III) onto $BaSO_4$·$CaSO_4$ composite [C_o = 1100 mg g^{-1}, Time = 20 min, pH = 4 and v/m = 0.2 L $g.^{-1}$]

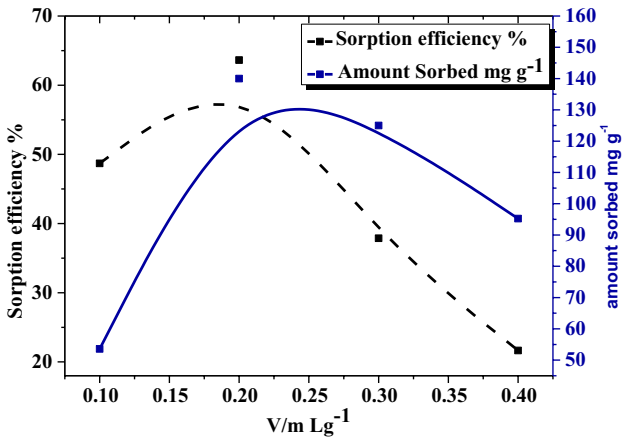

Fig. 9 V/m impact of sorption of REE (III) onto $BaSO_4$· $CaSO_4$ composite at 303 K [C_o = 1100 mg $g.^{-1}$, Time = 20 min, pH = 4 and Temp. = 303 K]

1st order is higher and closer to one. The values of the calculated capacity of the sorbed metal ions at equilibrium $q_{e(cal.)}$

Table 2 Kinetic modelling parameters for the sorption of REE(III) onto $BaSO_4$·$CaSO_4$ composite

		$BaSO_4$·$CaSO_4$ composite
Pseudo−first order		
q_e (mg g^{-1}) (calculated)		127.06
q_e (mg g^{-1}) (experiment)		140
K^1 (min^{-1})		0.151
R^2		0.991
Pseudo−second order		
q_e (mgg^{-1}) (calculated)		144.93
q_e (mgg^{-1}) (experiment)		140
K^2 (g mg^{-1} min^{-1})		0.003
R^2		0.998
Intraparticle diffusion		
K_{di1} (mg g^{-1} $min^{-1/2}$)	Time range 0–2 min	30.064
C (mg g^{-1})		1.147
R^2		0.95
K_{di2}	Time range 2− 15 min	26.5
C		25.94
R^2		0.93
K_{di3}	Time range 20− 120 min	–
C		140
R^2		–
Elovich kinetic model		
α (mg.g^{-1} min^{-1})		244.148
β (g.mg^{-1})		0.026
R^2		0.994

must match the experimental $q_{e(\text{exp.})}$ in all respect. The sorption reaction mechanism is suggested to follow a pseudo-2nd-order mechanism by comparing the estimated $q_{e(\text{cal.})}$ and observed $q_{e(\text{exp.})}$ values. This comparison also predicted a chemisorptions reaction [63].

The intercept (S.1c) ascribed to the thickness of the surface during interparticle-diffusion model evaluation revealed the participation of the surface adsorption in the rate-determining step. The larger the intercept, the more is its participation to the sorption reaction. The intra-particle diffusion model taken through three steps. The 1st step, which occurred within the first two minutes, represents the diffusion of metal ions from the solution to the surface of the $BaSO_4$·$CaSO_4$ composite. The second stage (from 3 to 15 min) was designed to simulate the gradual sorption of REE (III) on the surface onto $BaSO_4$·$CaSO_4$ composite may be the rate-determining step. The third stage (extended from 20 to 120 min) is the equilibrium saturation. The sorption reaction mechanism was controlled by multi-diffusion step.

The high correlation factor R^2 of Elvoich indicated that the sorption reaction was controlled by chemisorption mechanism with a confirmation to pseudo 2nd order fitting as the value of β (desorption constant) was very small compared to α (adsorption constant) [64].

Adsorption isotherm

To examine the fitting model to sorption reaction, Eqs. (10–14) were used. The parameters of the applied models were listed in Table 3. While S.2. a, b, c, and d depict the plots for the applied model; Langmuir, Freundlich, Halsey, and Temkin, respectively. The order of increase of correction factor was Langmuir > Halsey > Freundlich > Temkin. This order reflected the suitability of Langmuir model in describing the sorption of REE (III) onto $BaSO_4$·$CaSO_4$ composite. The sorption process was favourable because $R_L = 0.0654$, i.e. $0 < R_L < 1$.

Freundlich data results in Table 3 showed values of K_f and 1/n are 10.45 mg g^{-1} and 0.4161 ($n = 2.403$), respectively; the sorption was considered to be favourable because the freundlich exponent values of n were in the range (2–10) [65].

S.2. reflected a relatively good agreement of Halsey to the adsorption data with $R^2 = 0.96$ than the Freundlich isotherm; this result confirmed the heterogeneous nature of $BaSO_4$·$CaSO_4$ composite [65].

Applying Temkin isotherm model, $R^2 = 0.92$ and this model was not fit well to the equilibrium data compared to the Langmuir, Freundlich and Halsey. The calculated parameters A_T (1.005 L g^{-1}) was the equilibrium binding constant, which indicates the maximum bonding energy; b_T (176.534 kJ mol^{-1}) is the constant related to the heat of adsorption [66].

Table 3 Isotherm modelling parameters for the sorption of REE(III) onto $BaSO_4$·$CaSO_4$ composite

	$BaSO_4$·$CaSO_4$ composite
Langmuir isotherm parameters	
q_{max} (mg g^{-1})	168.63
b (L mg^{-1})	0.013
R_L	0.065
R^2	0.997
Freundlich isotherm parameters	
n	2.403
K_F (mgn^{-1} g^{-1} L^{-n})	10.45
R^2	0.958
Halsey isotherm parameters	
n_H	2.403
K_H	0.84
R^2	0.96
Temkin isotherm parameters	
A_T (L mg^{-1})	1.005
B_T	176.534 × 103
R^2	0.92

Table 4 Thermodynamic parameters of the sorption of REE(III) onto $BaSO_4$·$CaSO_4$ composite

Composite	ΔH kJmol^{-1}	ΔS Jmol^{-1} K^{-1}	ΔG kJmol^{-1}		
			Temperature (K)		
			303	313	323
$BaSO_4$·$CaSO_4$	38.783	176.70	−14.76	−16.43	−19.26

Thermodynamic studies

In S.3, a plot of ln K_d against 1/T for the sorption of REE (III) onto a combination of $BaSO_4$·$CaSO_4$ was shown. The parameters for thermodynamic studies were presented in Table 4. The free energy change ΔG^o obtained during the adsorption reaction at temperatures of 303, 313, and 323 K indicated that the adsorption of REE (III) onto $BaSO_4$·$CaSO_4$ composite was spontaneous and favourable. Additionally, increase in negative values of ΔG^o as temperature increased indicates greater driving force for binding of rare earth ions. The endothermic nature of the sorption process was confirmed by the positive value of ΔH^o. The positive value of ΔS^o was an evident for the affinity of REE (III) sorption onto $BaSO_4$·$CaSO_4$ composite due to the increase in randomness at the solid-solution interface during the adsorption process.

Desorption studies

Desorption experiments had been conducted to evaluate the ability of $BaSO_4$·$CaSO_4$ composite to release REE (III) ions using a variety of desorbing agents, including HNO_3, H_2SO_4, Citric acid, and distilled water. Figure 10a showed that the HNO_3 was the optimum desorbing agent for REE (III) sorbed onto $BaSO_4$·$CaSO_4$ with a Desorption efficiency 90.135%. The effect of increasing concentration of HNO_3 on the desorbing efficiency (Fig. 10b) implied that the desorbing efficiency increased with the increase in nitric acid concentration up to 1 mol L^{-1}. However, above 1 mol L^{-1} concentration of HNO_3, the desorbing efficiency was not changed. The difference in desorbing efficiency of HNO_3, H_2SO_4 and citric acid owing to the difference in acid strength where the order of increase of K_a is $H_2SO_4 > HNO_3 >$ citric acid $> H_2O$. However, an exception of the desorbing efficiency of HNO_3 is higher than that using H_2SO_4 due to the presence of SO_4^{2-} ions and common ion effect with $BaSO_4$·$CaSO_4$ leads to decrease the desorption of REE(III). In case of using distilled water as desorbing agent, the desorption efficiency was zero due to precipitation of REE (III) as RE $(OH)_3$. Comparatively higher REE(III) desorption from the $BaSO_4$·$CaSO_4$ composite was performed by increasing concentration of HNO_3 can be explained due to the increase of $[H^+]$ which results in the protonation of the surface of $BaSO_4$·$CaSO_4$ composite and electrostatic repulsion between REE (III) ions and $BaSO_4$·$CaSO_4$ composite [67].

Mechanism of sorption reaction

The mechanism of the sorption reaction was suggested to perform through three possible mechanisms as shown in Fig. 11; inclusion, occlusion, and adsorption. Inclusion was the process of replacing the main metal (Ba (II) or Ca (II)) in the crystalline structure with a REEs metal. Occlusion occurs when REEs are physically trapped between the layers of a growing mineral (i.e., $BaSO_4$ or $CaSO_4$), as evidenced by surface measurements and a decrease in porosity. Adsorption occurred at the surface when REEs were physically or chemically bound to the outer layer of $BaSO_4$·$CaSO_4$ [68]. The surface of $BaSO_4$·$CaSO_4$ composite was not electroneutral like the bulk of the composite due to the active surface SO_4^{2-} groups form incomplete coordination spheres, [68, 69]. Such a negatively charged surface has the potential to attract positively charged REE (III) ions from the liquor of monazite from surrounding solution, resulting in the formation of an electrical double layer (EDL) around

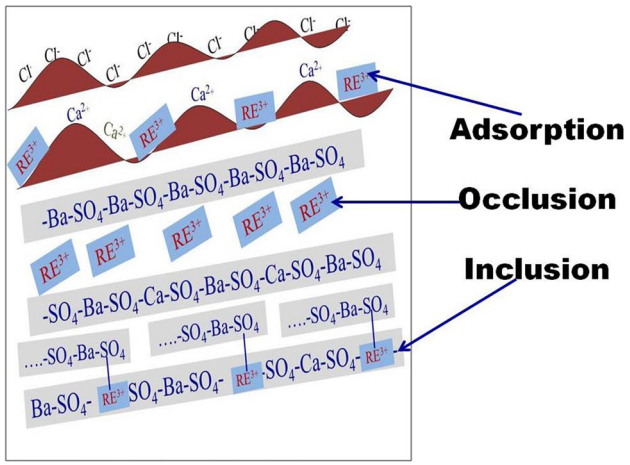

Fig. 11 Schematic diagram for the mechanism of sorption of REE (III) onto $BaSO_4$·$CaSO_4$ composite

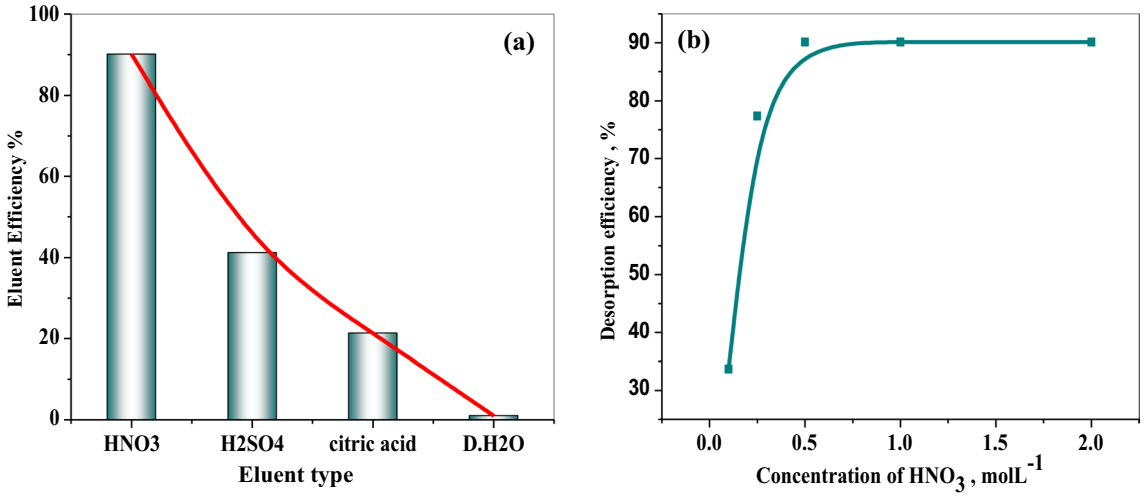

Fig. 10 Desorption study of REE (III) sorbed onto $BaSO_4$·$CaSO_4$ composite (a) using different eluents (b) different concentrations of HNO_3

$BaSO_4$·$CaSO_4$ composite. As a result, electrostatic interactions occurred.

The suggested mechanism could also be evaluated by measuring the concentration of Ca(II) released in the solution by ion exchange. This exchange related to high charge density that will favour the exchange with Ca(II) within $BaSO_4$·$CaSO_4$ layers [70]. Table 5 includes the initial and final concentrations of Ca(II) and REE(III) in the solution after sorption of REE(III) onto $BaSO_4$·$CaSO_4$ composite.

The LRE ions (light rare earth ions) have similar ionic radii to Ca (II) leads to high incorporation extent of LRE ions than HRE ions [71]. However, the charge difference between rare earth ions and Ca(II) limits the extent of the solid state substitution [71] where the Ca(II) released in solution was 488 mg L^{-1}; i.e. 19.52% of Ca(II) was substituted by rare earth ions [72].

Reusability

The efficiency of the $BaSO_4$·$CaSO_4$ composite was evaluated by regeneration and recycling of $BaSO_4$·$CaSO_4$ composite through (Adsorption–desorption-Adsorption) cycle. The desorbing agent was 1 mol L^{-1} HNO_3. The Sorbed amount of $BaSO_4$·$CaSO_4$ composite decreased after the first cycle from 140 to 103.4 mg g^{-1}. From the second cycle to fifth cycle, the sorption capacity was nearly 103 mg g^{-1} and not changed. i.e., the reusability of $BaSO_4$·$CaSO_4$ composite was 73.9%; this confirmed the suggested mechanism and nearly 74% of sorption was carried out by occlusion and adsorption. Figure 12 depicts the Adsorption–desorption-Adsorption cycles of $BaSO_4$·$CaSO_4$ composite for adsorption of REE (III) using 1 mol L^{-1} HNO_3.

Table 5 Initial and final concentrations of Ca (II) and REE (III) before and after sorption onto $BaSO_4$·$CaSO_4$ composite

Metal concentration	Ionic radius (Ao)	Initial concentration mg L^{-1}	Final concentration mg L^{-1}	Sorption efficiency %
Ca(II)	1.14	462	950	
La(III)	1.03	416.79	151.17	63.72
Ce(III)	1.01	518.13	188.18	63.68
Pr(III)	0.99	49.04	17.82	63.66
Nd(III)	0.98	91.83	33.44	63.58
Sm(III)	0.958	12.09	4.41	63.52
Eu(III)	0.947	0.54	0.197	63.51
Gd(III)	0.938	8.65	3.158	63.49
Tb(III)	0.923	0.76	0.277	63.47
Dy(III)	0.912	1.54	0.564	63.36
Ho(III)	0.901	0.27	0.099	63.33
Er(III)	0.89	0.36	0.1328	63.11
Tm(III)	0.88	0.02	0.00738	63.09
Yb(III)	0.868	0.06	0.0221	63.08
Lu(III)	0.86	0.005	0.00185	63
	Total	1100.13	399.47	63.68

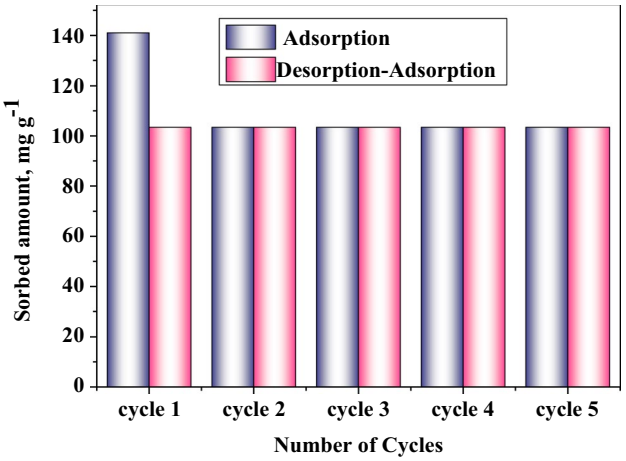

Fig. 12 Reusability of $BaSO_4$·$CaSO_4$ composite for adsorption of REE (III) using 1 M HNO_3

Sorption of REE (III) onto barite-gypsum composite

1:1 (*wt/wt*) Barite-gypsum composite (the natural ingredients for $BaSO_4$·$CaSO_4$ composite) was prepared by a physical mixing technique where barite and gypsum were crushed using an agate mortar, then thermally treated at 300 °C for 2 h with a rate of 5 °C min^{-1}. Then, the resulting mixture was grounded again before being used as an adsorbent. The previous sorption experimental results pointed to the efficient possibility of the use of barite. Gypsum composite in sorption of REE (III) digested solution. Table 6 illustrated the sorbed amounts of REE (III) on barite, gypsum, and barite-gypsum composite at the optimum conditional parameter determined during the previous experiments.

Conclusion

A synthetic $BaSO_4$·$CaSO_4$ composite was successfully prepared via the co-precipitation technique. Characterisation of $BaSO_4$·$CaSO_4$ composite was performed by FT-IR, XRD, DTA, SEM, particle size analysis, and pore size distribution. Adsorption of REEs elements from acidic aqueous solutions was examined using $BaSO_4$·$CaSO_4$ composite. The best adsorption parameters at 303 K of REEs ions were

Table 6 Sorbed amounts of RE(III) onto Barite, Gypsum, and Barite. Gypsum composite

Sorbent	Barite	Gypsum	Barite.Gypsum
Amount sorbed (mg g^{-1})	133	135	136

volume to composite mass ratio 0.2:1 L g^{-1}, pH = 4, initial concentration of REE sorbent; 1100 mg g^{-1}, and 20 min contact time. Kinetic and isotherm models were applied. The results indicated that, pseudo 2nd order model was more fitted. The adsorption mechanism was checked for Langmuir, Freundlich, Hasely, and Temkin isotherm models. Maximum adsorption capacity of rare earth ions onto the prepared $BaSO_4$·$CaSO_4$ composite was 168.63 mg g^{-1}. Thermodynamic studies showed the extent of adsorption capacity increases with temperature, i.e., the sorption reaction was endothermic and spontaneous. Desorption of REE (III) was performed using 1 mol L^{-1} HNO_3 with a desorption efficiency of 90.135%. The reusability of the $BaSO_4$·$CaSO_4$ composite was 73.9% for five successive adsorption –desorption-adsorptions cycles. The studied experimental results showed that we can use 1:1 (wt/wt) barite-gypsum composite; as natural ingredient for $BaSO_4$·$CaSO_4$ composite; for REE (III) sorption, barite-gypsum composite were prepared by physical mixing and thermally treated at 300 oC for 2 h as a host and cheap sorbent for rare earth ions. The amount of REE (III) that has been sorbed onto the barite-gypsum composite was 136 mg g^{-1}.

Supplementary Information The online version contains supplementary material available at https://doi.org/10.1007/s10967-022-08669-4.

Author contributions All authors contributed to the study conception and design, Material preparation, data collection and analysis. All authors read and approved the final manuscript.

Funding Open access funding provided by The Science, Technology & Innovation Funding Authority (STDF) in cooperation with The Egyptian Knowledge Bank (EKB). The authors received no financial support for the research, authorship, andor publication of this article.

Data Availability All the data used for this work are publicly available.

Declarations

Conflict of interest The authors declare that they have no conflict of interest.

Consent to participate All of the authors consented to participate in the drafting of this manuscript.

Consent for publication All of the authors consent to publish this manuscript.

Ethical approval.
The authors confirm that the manuscript has been read and approved by all authors. The authors declare that this manuscript has not been published and not under consideration for publication elsewhere.

Human and animals Not applicable.

References

1. Balaram V (2019) Rare earth elements: a review of applications, occurrence, exploration, analysis, recycling, and environmental impact. Geosci Front 10:1285–1303
2. Hosshino M, Sanematsu K, Watanabe Y (2016) Handbook on the Physics and Chemistry of Rare Earths. 49: chapter 279 REE mineralogy and resource, J.-C.G. Bunzil and V.K. Pecharsky
3. William Boynton V, Douglas Brookins G, Donald Brutm M, Larry Haskin A, Anthony Mariano N et al (1989) Geochemistry and Mineralogy of Rare Earth Elements. BR, Lipin, GA McKay. Walter de Gruyter GmbH and Co.KG, Berlin, pp 21–29
4. Goodenough KM, Wall F, Merriman D (2018) The rare earth elements: demand, global resources, and challenges for resourcing future generations. Nat Res Res 27:201–216
5. James BH, Labiba W (1989) Heavy minerals, including monazite, in Egypt's black sand deposits. J Less Common Metals 148:79–84
6. Han KN (2020) Characteristics of precipitation of rare earth elements with various precipitants. Minerals 10:178
7. Nascimento M, Valverde B, Ferreira F, Gomes R, Soares PS (2015) Separation of rare earths by solvent extraction using DEHPA Rem. Rev Escola de Minas 68:427–434
8. Rychkov V, Kirillov E, Kirillov S, Bunkov G, Mashkovtsev M, Botalov M, Semenishchev V, Volkovich V (2016) Selective ion exchange recovery of rare earth elements from uranium mining solutions. AIP Conf Proc 1767:020017
9. Ioannis A, Amit B, Eder CL (2016) Adsorption of rare earth metals: a review of recent literature. J Mol Liquids 221:76
10. Meilinda H, Husein HB, Anggraeni A, Syulastri E (2021) Preparation of liquid emulsion membranes for separation of Gadolinium (III) from samarium (III) with tributyl phosphate or Di-(2-Ethylhexyl) phosphoric acid extraction based on emulsion stability. Chem Sci J 12:10–26
11. Davoodi-nasab P, Rahbar-Kelishami A, Safdari J, Abolghasemi H (2018) Evaluation of the emulsion liquid membrane performance on the removal of gadolinium from acidic solutions. J Mol Liqu 262:97–103
12. Tang C, Bruening ML (2020) Ion separations with membranes. J Poly Sci 58:2831–2856
13. Silva RG, Morais CA, Teixeira LV, Oliveira LV, Eder D (2019) Selective Precipitation of high-quality rare earth oxalates or carbonates from a purified sulfuric liquor containing soluble impurities. Min Metall Explorat 36:967–977
14. Gergoric M, Barrier A, Retegan T (2019) Recovery of rare-earth elements from neodymium magnet waste using glycolic, maleic, and ascorbic acids followed by solvent extraction. J Sustain Metall 5:85–96
15. Hagag MS, Morsy AMA, Ali AH (2019) Adsorption of rare earth elements onto the phosphogypsum a waste byproduct. Water Air Soil Pollut 230:1–14
16. Felipe ECB, Batista KA, Ladeira ACQ (2021) Recovery of rare earth elements from acid mine drainage by ion exchange. Environ Technol 42:2721–2732
17. Kazuya U, Masahiro G, Shinji I, Kiyoshi I, Fumiyuki N (1995) Extraction of rare earth metals using liquid surfactant membranes prepared by a synthesized surfactant. Separat Sci Technol 30:3325–3338

18. Chen L, Dong H, Pan W, Dai J, Dai X, Pan J (2021) Poly (vinyl alcohol-co-ethylene)(EVOH) modified polymer inclusion membrane in heavy rare earths separation with advanced hydrophilicity and separation property. Chem Eng J 426:131305
19. Renata AD, Morais A, Carlos MA (2010) Purification of rare earth elements from monazite sulphuric acid leach liquor and the production of high-purity ceric oxide. Miner Eng 23:536–540
20. Lokshin EP, Tareeva OA, Elizarova IR (2011) Deposition of rare earth elements from a wet-process phosphoric acid by fluorine compounds. Russ J Appl Chem 84:773–781
21. Worch E (2021) Adsorption technology in water treatment: fundamentals, processes, and modelling. De Gruyter, Berlin, Boston, pp 1–40
22. Biswas FB, Rahman IMM, Nakakubo K, Endo M (2021) Highly selective and straight forward recovery of gold and platinum from acidic waste effluents using cellulose-based bio-adsorbent. J Hazard Mater 410:124569
23. Yi W, Yuan-ping G, Hong-xia L, Ru-yi Zhou Z, Jun-xia Y, Haobo H, Weiyan Y, Ru-An C (2021) Sequential recycle of valuable phosphorus compounds of glyphosine, glyphosate, and phosphorous acid from glyphosate mother liquor by D301 resin through sorbent dosage control. J Environ Chem Eng 9:106474
24. Tkachenko I, Tkachenko NS, Ekaterina LS, Nadezhda MA, Valery LV (2020) Two-stage Ozonation–adsorption purification of ground water from trichloroethylene and tetrachloroethylene with application of commercial carbon adsorbents. Ozone: Sci Eng 42: 357–370. doi 10.108001919512.2020.1735994
25. Heidari A, Sayadi MH, Biglari Quchan Atigh Z (2021) A comparative study of different materials (drinking water treatment sludge, nanoclay, and modified nanoclay) for simultaneous removal of hexavalent chromium and lead. Int J Environ Sci Technol 18:3553–3570
26. Rashed MN, Palanisamy PN (2018) Introductory chapter: adsorption and ion exchange properties of zeolites for treatment of polluted water. Zeol Their Appl 10:70980
27. Feng X, Onel O, Council-Troche M, Noble A, Yoon RH, Morris JR (2020) A study of rare earth ion-adsorption clays: the speciation of rare earth elements on kaolinite at basic pH. Appl Clay Sci 201:105920
28. Ji B, Zhang W (2021) The effect of mechanical grinding and thermal treatment on the recovery of rare earth elements (REEs) from kaolinite. Powder Technol 394:622–631
29. Yang M, Liang X, Ma L, Huang J, He H, Zhu J (2019) Adsorption of REEs on kaolinite and halloysite: a link to the REE distribution on clays in the weathering crust of granite. Chem Geology 525:210–217
30. Nkinahamira F, Alsbaiee A, Wang Y, Yang X, Chen T-Y, Cao M, Feng M, Sun Q, Yu C-P (2021) Recovery and purification of rare earth elements from wastewater and sludge using a porous magnetic composite of β-cyclodextrin and silica doped with PC88A. Separat Purificat Technol. 266:118589
31. Zhao X, Jiang X, Peng D, Teng J, Yu J (2021) Behavior and mechanism of graphene oxide-TRIS (4-aminophenyl) amine composites in adsorption of rare earth elements. J Rare Earths 39:90–97
32. Ali AH, Dakroury GA, Hagag MS, Abdo SHM, Allan KF (2022) Sorption of some rare earth elements from acidic solution onto poly (acrylic acid–co-acrylamide16, 16-dimethylheptadecan-1-amine) composite. J Polym Environ 30:1170–1188
33. Lin W, Zhao Z, Yang F, Liu Z, Tan F, Xie M, Ma Y, Meng L (2021) Promising priority separation of europium from lanthanide by novel DGA-functionalized metal organic frameworks. Minerals Eng 164:106831
34. Abdel-Magied AF, Abdelhamid HN, Ashour RM, Zou X, Forsberg K (2018) Hierarchical porous zeolitic imidazolate frameworks nanoparticles for efficient adsorption of rare-earth elements. Microp Mesop Mater 278:175–184
35. He C, Salih KAM, Wei Y, Mira H, Abdel-Rahman AA-H, Elwakeel KZ, Hamza MF, Guibal E (2021) Efficient recovery of rare earth elements (Pr(III) and Tm(III)) from mining residues using a new phosphorylated hydrogel (Algal Biomass PEI). Metals 11:294
36. Byron L, Bou JJ, Hoyo J, Carrillo M, Peña K, Tzanov T, Sastre AM (2020) A potential lignocellulosic biomass based on banana waste for critical rare earths recovery from aqueous solutions. Environ Pollut 264:114409
37. McLellan BC, Corder GD, Ali SH (2013) Sustainability of rare earths—an overview of the state of knowledge. Minerals 3:304–317
38. Binnemans K, Jones PT, Blanpain B, Gerven TV, Yang Y, Walton A, Buchert M (2013) Recycling of rare earths: a critical review. J Clean Product 51:1–22
39. Innocenzi V, Michelis ID, Kopacek B, Vegliò F (2014) Yttrium recovery from primary and secondary sources: a review of main hydrometallurgical processes. Waste Manage 34:1237–1250
40. Dakroury GA, Allan KF, Attallah MF, El Afifi EM (2020) Sorption and separation performance of certain natural radionuclides of environmental interest using silicaolive pomace nanocomposites. J Radioanalyt Nucl Chem 325(2):625–639
41. Azazaa H, Doggaza A, Mechia L, Optasanub V, Tlilia M, Ben Amor M (2017) Synthesis of intermediate crystal $Ba_{1-x}Ca_x SO_4$ system via co-precipitation of $BaSO_4$ -$CaSO_4$ and partial hindrance of gypsum formation. Desalinat Water Treat J 66:80–87
42. Dakroury GA, El-Shazly EAA, Hassan HS (2021) Preparation and characterization of ZnO Chitosan nanocomposite for Cs(I) and Sr(II) sorption from aqueous solutions. J Radioanal Nucl Chem 330:159–174
43. El-Shazly EAA, Dakroury GA, Someda HH (2021) Sorption of ^{134}Cs radionuclide onto insoluble ferrocyanide loaded silicagel. J Radioanal Nucl Chem 329:437–449
44. El-Shazly EAA, Dakroury GA, Someda HH (2021) Kinetic and isotherm studies for the sorption of ^{134}Cs and ^{60}Co radionuclides onto supported titanium oxide. J Radioanalyt Nucl Chem 330(1):127–139
45. Weber WJ, Morris JC (1963) Kinetics of adsorption on carbon from solution. J Sanit Eng Div, Am Soc Civ Eng 89:31–60
46. Langmuir I (1918) The adsorption of gases on plane surfaces of glass, mica and platinum. J Am Chem Soc 40:1361–1403
47. Weidner E, Ciesielczyk F (2019) Removal of hazardous oxyanions from the environment using metal-oxide-based. Materials 12:109
48. Ayawei N, Ebelegi AN, Wankasi D (2017) Modelling and Interpretation of adsorption isotherms. J Chem 20:17
49. Vijayaraghavan K, Padmesh TVN, Palanivelu K, Velan M (2006) Biosorption of nickel(II) ions onto sargassum wightii: application of two-parameter and three-parameter isotherm models. J Hazard Mater 133:304–308
50. Ayanda FA, Anuar MFM, Zaibon S, Jusop S (2021) The physicochemical and mineralogical characterization of mg-rich synthetic gypsum produced in a rare earth refining plant. Sustainability 13:4840
51. Ramaswamy V, Vimalathithan RM, Ponnusamy V (2010) Synthesis and Characterization of $BaSO_4$ Nano-particles Using Microemulsion Technique. Adv Appl Sci Res 1:409
52. Li S, Zheng L, Yu L (2011) Preparation of flower-shaped barium sulfate nanoparticles in the presence of DTAB. J Dispers Sci Technol 32:601–603
53. Qiaoshan C, Luchao W, Yaxiong Z, Caiyun J, Junming L, Matthew ZY, Baohong G (2019) Formation of spherical calcium sulfate mesocrystals: orientation controlled by subunit growth. Cryst Eng Comm 21:5973–5979
54. Hah M, Badwaik V, Kherde Waghwani HK, Modi T, Aguilar ZP, Rodgers H, Hamilton W, Marutharaj T, Webb C, Lawrenz MB, Dakshinamurthy R (2014) Gold nanoparticles: various methods of

synthesis and antibacterial applications. Front Biosci (Landmark Ed) 19:1320–1344
55. Zhou Z, Mitchell CA, Buchanan FJ, Dunne NJ (2013) Effects of heat treatment on the mechanical and degradation properties of 3D-printed calcium-sulphate-based scaffolds. ISRN Biomater doi 10:540
56. Lu H, Zhang Q, Dong Y, Li J, Zhang X (2016) The adsorption capacity, pore structure, and thermal behavior of the modified clay containing SSA. Adv Mater Sci Eng 20:16–17
57. Devanathan R, Balaji GL, Lakshmipathy AUR (2021) Adsorption of Rare Earth Ce^{3+} and Pr^{3+} Ions by Hydrophobic Ionic Liquid. J Environ Public Health 20:21
58. Shukla J, Mohandas VP, Kumar A (2008) Effect of pH on the solubility of $CaSO_4{\cdot}2H_2O$ in aqueous NaCl solutions and physicochemical solution properties at 35 °C. J Chem Eng Data 53:2797–2800
59. Kumar PS, Vincent C, Kirthika K, Kumar KS (2010) Kinetics and equilibrium studies of Pb^{2+} in removal from aqueous solutions by use of Nano-Silversol-coated activated carbon. Brazil J Chem Eng. 27:339–346
60. Badessa TS, Wakuma E, Yimer AM (2020) Bio-sorption for effective removal of chromium(VI) from wastewater using Moringa stenopetala seed powder (MSSP) and banana peel powder (BPP). BMC Chem 14:1–29
61. Abdulaziz A, Abdel-Basit A, Waseem S, Abdullah A, Fahad A, Taieb A (2019) Efficient adsorption of lead (II) from aqueous phase solutions using Polypyrrole-based activated carbon. Materials 12:119
62. Igberase E, Osifo P, Ofomaja A (2017) The adsorption of Pb, Zn, Cu, Ni, and Cd by modified ligand in a single component aqueous solution: equilibrium, kinetic, thermodynamic, and desorption studies. Int J Analyt Chem. 10:11
63. Igberase E, Osifo P (2015) Equilibrium, kinetic, thermodynamic and desorption studies of cadmium and lead by polyaniline grafted cross-linked chitosan beads from aqueous solution. J Indust Eng Chem 26:340–347
64. Hassan HS, Attia LA, Dakroury GA (2020) Exploration of the parameters affecting the radioactive europium removal from aqueous solutions by activated carbon-epoxy composite. Appl Radiat Isotopes 164:109278
65. Uduakobong E, Augustine I (2020) Kinetics, isotherms, and thermodynamic modeling of the adsorption of phosphates from model wastewater using recycled brick waste. Processes 8:665
66. Amin MT, Alazba AA, Shafiq M (2015) Adsorptive removal of reactive black 5 from wastewater using bentonite clay: isotherms, kinetics and thermodynamics. Sustainability 7:15302–15318
67. Paluri P, Ahmad KA, Durbha KS (2020) Importance of estimation of optimum isotherm model parameters for adsorption of methylene blue onto biomass derived activated carbons: comparison between linear and non-linear methods. Biomass Convers Bioref 105:201
68. Shah I, Adnan R, Wan Ngah WS, Mohamed N (2015) Iron impregnated activated carbon as an efficient adsorbent for the removal of methylene blue: regeneration and kinetics studies. PLoS ONE 10:e0122603
69. Harvey D (2000) Modern analytical chemistry. McGraw-Hill, New York
70. Bokern DG, Hunter KA, McGrath KM (2003) Charged barite− aqueous solution interface: surface potential and atomically resolved visualization. Langmuir 19:10019–10027
71. Cristiani C, Bellotto M, Dotelli G, Latorrata S, Ramis G, Stampino PG, Zubiani EMI, Finocchio E (2020) Rare Earths (La, Y, and Nd) adsorption behaviour towards mineral clays and organoclays: monoionic and trionic solutions. Minerals 11:109
72. Dutrizac JE (2017) The behaviour of the rare earth elements during gypsum (CaSO4·2H2O) precipitation. Hydrometallurgy 174:38–46